SCIENTIFIC OASIS

Spectrum of Mechanical Engineering and Operational Research

Journal homepage: www.smeor-journal.org
eISSN: 3042-0288


# Enhanced Thermal Study in Hybrid Nanofluid Flow through a Channel Motivated by Water/Cu+$Al_2o_3$ and Entropy Generation

Zaheer Abbas[1], Muhammad Yousuf Rafiq[1], Jafar Hasnain[2,*], Ghulam Mustafa[1], Muhammad Shakib Arslan[1]

[1] Department of Mathematics, The Islamia University of Bahawalpur, Bahawalpur, Pakistan
[2] Department of Computer Science, Bahria University, Islamabad, Pakistan

**ARTICLE INFO**

***Article history:***
Received 1 March 2024
Received in revised form 24 July 2024
Accepted 27 July 2024
Available online 30 July 2024

***Keywords:***
Oscillatory flow; hybrid nanofluid; MHD; thermal radiation; entropy generation; analytical solution.

**ABSTRACT**

This study examines the analysis of entropy generation in the magnetohydrodynamic oscillatory convective flow of hybrid nanofluid through a porous horizontal channel with velocity slip. The analysis incorporates suction at the cold wall and injection at the hot wall. Variable viscosity, thermal radiation, and viscous dissipation are also considered. Utilizing similarity transformations, the governing nonlinear partial differential equations are converted into ordinary differential equations, and exact solutions are obtained using Mathematica. Graphs are used to illustrate the impact that a variety of physical factors have on velocity, temperature, entropy generation, the Bejan number, skin friction, and the Nusselt number. The graphic results demonstrate that the fluid velocity is positively correlated with the cold wall slip parameter and negatively correlated with the hot wall slip parameter. There is an opposite relationship between fluid temperature and thermal radiation and an ascending relationship between fluid temperature and the Brinkman number. Findings from this study have important implications for better thermal management, device performance, and reliability as well as for optimizing microelectronic cooling systems.

## 1. Introduction

Channel flow with oscillation has extensive and far-reaching applications in several fields such as environmental science, medicine, engineering and fluid dynamics research. It can regulate the flow properties without making any changes to the system's physical framework or channel, which makes it versatile and practical in many contexts. Flow conditions can also be optimized and reduced energy consumption can be achieved in heat exchangers and reactors due to oscillatory flow. Biochemical tests, medical diagnostics, and chemical analysis are some microfluidic devices which can benefit from oscillatory flow. Makinde and Mhone [1] showed that magnetohydrodynamics and radiative heat transfer have a significant influence on the heat distribution and dynamics of oscillatory flow in

* *Corresponding author.*
*E-mail address: jafar_hasnain14@yahoo.com*

https://doi.org/10.31181/smeor1120249

a channel with porous walls. Navier slip and hydromagnetic oscillatory flow in porous channels were studied by Mahmoud and Ali [2]. With the use of an analytical solution, Abdul-Hakeem and Sathiyanathan [3] were able to determine the two-dimensional oscillatory flow of an incompressible viscous fluid in an extremely porous material that is contained by an infinite vertical plate. Fluid flow properties under these conditions are important for engineering applications, and their research improves our understanding of them. Jha and Ajibade [4-6] contributed significant insights into the dynamics of fluid flow and heat transfer by studying oscillatory flows affected by time-dependent boundary conditions. Their research enhanced the understanding of convective processes. Umavathi et al. [7] examined the heat transfer properties in the oscillatory flow of a viscous liquid through a composite channel that is oriented horizontally. Yuan and Wang [8] found that acceleration skewness affects vortex formation in oscillatory tunnels, with different vortices forming in each half period, significantly impacting sediment transport and aiding vortex dynamics understanding. Earnshaw and Greated [9] validated a discrete vortex model by studying periodic changes in vortex characteristics on ripples under oscillatory flow and waves, enhancing the understanding of vortex-surface interactions. Their findings offer valuable insights into both natural and engineered environments. Malarkey and Davies [10] and Chen and Yu [11] highlighted the critical role of periodic vortex structures in boundary layer development and sediment transport, despite varying definitions of vortex parameters. Their findings enhance predictions of sediment movement and boundary layer dynamics in aquatic environments. Hu et al. [12] analyzed hydrodynamic forces on partially submerged cylinders in the presence of both constant and oscillatory flow. They measured the forces of drag, lift, and inertia. Their discoveries offer a vital understanding of the interplay between flow regimes and their influence on marine structures. Ja'fari and Jaworski [13] studied nonlinear flow behavior in high-pressure standing-wave thermoacoustic heat engines, providing insights to optimize performance and efficiency. Niyas and Shajia investigated the use of biodiesel in a diesel engine after its production [14]. Anasuya and Srinivas [15] investigated the impact of magnetohydrodynamic (MHD) two-fluid oscillatory flow on heat transport in a tilted, fully saturated porous channel, with potential implications for engineering purposes.

Research by Choi and Eastman [16] presented that adding metallic nanoparticles to conventional fluids significantly improves thermal conductivity, which in turn improves the efficiency of heat transfer systems. This modification allows rapid and effective heat dispersion in critical applications which include industrial heat exchangers, radiators in vehicles and electronic cooling systems. Consequently, these systems experience enhanced performance and energy efficiency. Kirubadurai et al. [17] determined that the augmentation of nanoparticle volume fraction and the use of spherical nanoparticles have a substantial impact on improving heat transfer in nanofluids. The efficiency of this enhancement is impacted by the Reynolds number. Bang and Chang [18] conducted an experimental investigation to investigate heat transmission in water nanofluids. They observed a decrease in heat transfer during pool nucleate boiling situations. In their study, Nallusamy et al. [19] discovered that certain parameters considerably enhance thermal conductivity in nanofluids when the concentration of nanoparticles is low. This research proves that nanofluids can be used to cool systems with a high heat flux. To determine whether hybrid nanofluids could be useful for cooling systems and thermal management, Suresh et al. [20] investigated their improved thermal and physical characteristics. The use of water-based hybrid nanofluids improves thermal management and performance, according to research by Hayat and Nadeem [21]. These nanofluids also drastically improve heat transfer and temperature distribution in sheets that are stretched in a linear fashion. The efficacy of hybrid nanofluids as coolants in heat exchangers can be improved by increasing the concentration of nanoparticles up to 1%, according to research by Madhesh and Kalaiselvam [22]. A

study conducted by Ahmadi et al. [23] investigated the impact of nanoparticle size and structure on the thermal conductivity of nanofluids. Subhani and Nadeem [24] did a numerical investigation on heat transfer utilizing hybrid nano-fluids, emphasizing a substantial enhancement in heat transmission in comparison to standard nanofluids [25-26].

Systems such as microfluidic devices and nano-scale channels are affected by the slip boundary condition, which is essential for comprehending fluid interactions at solid interfaces. For accurate modeling in cases where fluid-solid interactions are critical, like thin fluid films, it is important. The compatibility of nonlinear terms with slip circumstances must be carefully considered to address the complexity of these conditions, particularly in compressible MHD systems. Tang and Gao [27] studied local strong solutions to the compressible MHD equations with an initial vacuum and slip condition, enhancing the theoretical understanding of such fluid behaviors. Xi and Hao [28] demonstrated the local existence of classical solutions for the fully compressible MHD system under slip boundary conditions, but global existence for general conditions remains unresolved. Cai and Li [29] proved the global existence of classical solutions for barotropic compressible Navier-Stokes equations in bounded domains with slip boundary conditions, overcoming previous challenges using new techniques for a priori and boundary estimates.

Based on the literature survey, the analysis of slip conditions and non-uniform wall temperatures on thermal conductivity and heat transfer radiation in hybrid nanofluid flows through a porous horizontal channel has not yet been reported. Therefore, we investigate the entropy generation in magnetohydrodynamic oscillatory convective flow of a hybrid nanofluid through a porous horizontal channel with velocity slip. Similarity transformation converts nonlinear PDEs to ODEs, solved using Mathematica. The effects of various physical parameters on flow variables are illustrated through graphs and tables. The findings offer practical applications for designing efficient cooling systems in electronic devices by optimizing velocity slip and wall temperature distribution to enhance heat transfer and improve device performance.

## 2. Problem Formulation

Consider an unsteady incompressible laminar flow of hybrid nanofluid passing through a channel of non-uniform wall temperature. A magnetic field $B_0$ is exerted in the normal direction of the channel. The lower and the upper walls are conserved at constant temperature $T_0$ and $T_1$ within the channel. The lower wall resembles suction and the upper wall is under the action of blowing. The center of the channel was denoted by $x'$ and $y'$ shows the distance along the regular section such that $y'=a$ shows half of the width of the current channel in the Rectangular coordinate system ($x'$, $y'$)shown in Figure 1.

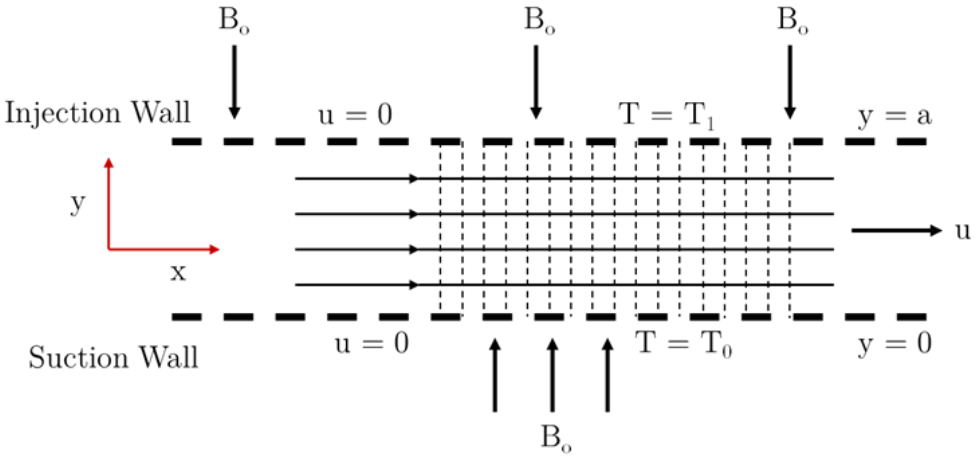


**Fig. 1.** Flow geometry

The fundamental equations of fluid flow dynamics can be written as

$$\nabla \bullet \boldsymbol{V} = 0, \tag{1}$$

$$\rho_{hnf}\left(\boldsymbol{V} \bullet \nabla \boldsymbol{V} + \frac{\partial \boldsymbol{V}}{\partial t}\right) = \boldsymbol{J} \times \boldsymbol{B} - \nabla \boldsymbol{p} + \mu_{hnf} \nabla^2 \boldsymbol{V}, \tag{2}$$

$$\left(\rho C_P\right)_{hnf}\left(\boldsymbol{V}.\nabla \boldsymbol{T} + \frac{\partial \boldsymbol{T}}{\partial t}\right) = k_{hnf} \nabla^2 \boldsymbol{T} + \Phi - \frac{\partial q_r}{\partial y}, \tag{3}$$

where μ describes the dynamic viscosity, ρ designates the density, ***B*** implies magnetic field strength, **J** denotes the current density, *k* symbolizes the thermal conductivity, and $C_p$ is the specific heat at constant pressure.

The viscous dissipation term is described by the expression [19]:

$$\Phi = 2\mu_{hnf}\left\{\left(\frac{\partial u}{\partial x}\right)^2 + \left(\frac{\partial v}{\partial y}\right)^2 + \left(\frac{\partial w}{\partial z}\right)^2\right\} + \mu_{hnf}\left[\left(\frac{\partial u}{\partial y} + \frac{\partial v}{\partial x}\right)^2 + \left(\frac{\partial w}{\partial y} + \frac{\partial v}{\partial z}\right)^2 + \left(\frac{\partial u}{\partial z} + \frac{\partial w}{\partial x}\right)^2\right], \tag{4}$$

Rosseland approximation calculates radiative heat flux in thick media as follows

$$q_r = -\frac{4\sigma^*}{3k^*}\frac{\partial T^4}{\partial y}, \tag{5}$$

where the Stefan-Boltzmann constant and the mean absorption coefficient are $k^*$ and $\sigma^*$, respectively. Within the flow, thermal differences are supposed to be very small so that the linear function of the temperature $T^4$ can be expanded in a Taylor series about $T_0$, and the higher terms are neglected, one obtains

$$T^4 = 4T_0^3 T - 3T_0^4. \tag{6}$$

The structure of the unsteady velocity flow field is as follows.

$$\boldsymbol{V} = \left(u\left(y,t\right),0,0\right). \tag{7}$$

Ohm's law defines the current density vector as:

$$\boldsymbol{J} = \sigma_{hnf}\left(0,0,B_0 u\right). \tag{8}$$

It is possible to compute the resistive Lorentz force as

$$\boldsymbol{J} \times \boldsymbol{B} = \sigma_{hnf}\left(-B_0^2 u,0,0\right). \tag{9}$$

The governing equations of nanofluid with suction/injection are as follows based on the previously mentioned assumptions:

$$\frac{\partial u'}{\partial t'} = -\frac{1}{\rho_{hnf}}\frac{dP'}{dx'} + \nu_{hnf}\frac{\partial^2 u'}{\partial y'^2} - \frac{\nu_{hnf}}{K}u' - \frac{\sigma_{hnf}B_0^2 u'}{\rho_{hnf}}, \tag{10}$$

$$\frac{\partial T'}{\partial t'} = \frac{k_{hnf}}{\left(\rho C_p\right)_{hnf}}\left(1 + \frac{16\sigma^* T_0^3}{3k^* k}\right)\frac{\partial^2 T'}{\partial y'^2} + \frac{\mu_{hnf}}{\left(\rho C_p\right)_{hnf}}\left(\frac{\partial u'}{\partial y'}\right)^2, \tag{11}$$

subjected to the boundary conditions

$$\begin{aligned} u' &= \left(\phi'\right)\frac{du'}{dy'} \;\; ; \quad T' = T_0, \quad y' = 0, \\ u' &= \left(\phi''\right)\frac{du'}{dy'} \;\; ; \quad T' = T_1, \quad y' = a. \end{aligned} \tag{12}$$

Where *t′* is time, *K* is porous permeability, $B_0$ denotes the magnetic field's strength, ϕ′ and ϕ′′ are the slip parameters because of the porous medium. The thermophysical properties given in Table 1 and Table 2, including $(\rho C_p)_{hnf}$ the heat capacity of the hybrid nanofluid, $\rho_{hnf}$ show the density of the

hybrid nanofluid, $\mu_{hnf}$ denotes the usual dynamic viscosity of the hybrid nanofluid, and $k_{hnf}$ is the thermal conductivity of hybrid nanofluid which is defined as:

**Table 1**
Thermophysical relations of alumina-copper/water and copper/water nanofluids

| **Property** | **Hybrid nanofluid** | **Nanofluid** |
|---|---|---|
| Dynamic viscosity | $\mu_{hnf} = \frac{\mu_{nf}}{(1-\phi_2)^{2.5}}$ | $\mu_{nf} = \frac{\mu_f}{(1-\phi_1)^{2.5}}$ |
| Density | $\rho_{hnf} = (1-\phi_2)\rho_{nf} + \rho_{S_2}\phi_2$ | $\rho_{nf} = (1-\phi_1)\rho_f + \rho_{S1}\phi_1$ |
| Heat capacity | $(\rho C_p)_{hnf} = (\rho C_p)_{nf}(1-\phi_2) + \phi_2\rho_{S_2}C_{pS_2}$ | $(\rho C_p)_{nf} = (1-\phi_1)(\rho C_p)_f + \phi_1\rho_{S_2}C_{pS_2}$ |
| Thermal conductivity | $\frac{k_{hnf}}{K_{nf}} = \left(\frac{2k_{nf} + k_{S_2} - 2(-k_{S_2} + k_{nf})\phi_2}{2k_{nf} + k_{S_2} + (-k_{S_2} + k_{nf})\phi_2}\right)$ | $\frac{k_{nf}}{k_f} = \left(\frac{k_{S_1} + k_f 2 - 2(-k_{S_1} + k_f)\phi_1}{k_{S_1} + k_f 2 + (-k_{S_1} + k_f)\phi_1}\right)$ |
| Electrical conductivity | $\sigma_{hnf} = \sigma_{nf}\left(\frac{2(1-\phi_2)\sigma_f + (2\phi_2+1)\sigma_{S2}}{(2+\phi_2)\sigma_f + (-\phi_2+1)\sigma_{S2}}\right)$ | $\frac{\sigma_{nf}}{\sigma_f} = \left(\frac{2\sigma_f(1-\phi_1) + (2\phi_1+1)\sigma_{S_1}}{\sigma_f(2+\phi_1) + (-\phi_1+1)\sigma_{S_1}}\right)$ |

**Table 2**
Thermophysical attributes of copper, alumina, and water

| Base fluid and Nano-particles | $\rho$ $(kg/m^3)$ | $C_p$ $(1/kg\,k)$ | $k$ $(W/m\,k)$ |
|---|---|---|---|
| $H_2O$ | 997.1 | 4179 | 0.6130 |
| $Cu\ (S_1)$ | 8933 | 385 | 400 |
| $Al_2O_3\,(S_2)$ | 3970 | 765 | 40 |

Where the subscripts $S$ represent the nano solid particles, $f$ denote the base fluid, $nf$ show the thermophysical properties of nanofluid, and $hnf$ show the hybrid nanofluid.

Dimensionless quantities are specified by

$$(x,y) = \frac{1}{h}(x',y'),\ u = \frac{u'h}{\nu_f},\ t = \frac{\nu_f t'}{h^2},\ p = h^2\left(\frac{p'}{\rho_f {\nu_f}^2}\right),\ \theta = \frac{T'-T_0}{T_1-T_0},\ \lambda = -\frac{dp}{dx}. \tag{13}$$

Substituting the dimensionless parameters in Equation (10)-(12), we get

$$\frac{\partial u}{\partial t} = -\frac{1}{A_1}\frac{dP}{dx} + \frac{A_2}{A_1}\frac{\partial^2 u}{\partial y^2} - \frac{1}{Da}u\frac{A_2}{A_1} - \frac{A_3}{A_1}H^2 u, \tag{14}$$

$$\frac{\partial \theta}{\partial t} = \alpha\frac{\partial^2\theta}{\partial y^2} + \beta Br\left(\frac{\partial u}{\partial y}\right)^2, \tag{15}$$

The simplified boundary conditions are

$$u(0) = \gamma\frac{du}{dy}(0),\quad \theta(0) = 0,\quad u(1) = \sigma\frac{du}{dy}(1),\quad \theta(1) = 1. \tag{16}$$

Where $A_1 = \rho_{hnf} / \rho_f$, $A_2 = \mu_{hnf} / \mu_f$, $A_3 = \sigma_{hnf} / \sigma_f$, $A_4 = \left(\rho C_p\right)_{hnf} / (\rho C)_f$, $A_5 = K_{hnf} / K_f$, $H^2 = \sigma_e B_0{}^2 h^2 \big/ \rho_f \nu_f$ Hartmann's number, $Br = \mu_f u^2 \big/ k_f \left(T_0 - T_1\right)$ and Brinkman's number, $S^2 = 1/Da$ denote the thermal conductivity parameter, whereas, $Da = K \big/ h^2$, $\alpha = A_5 \big/ A_4 * \Pr + Rd \big/ A_4 * \Pr$ and $\beta = A_2 \big/ A_4$. $\Pr = \rho_f C_{pf} \nu_f \big/ k$ is Prandtl number, $Rd = 16\sigma^* T_0^3 \big/ 3k^* k$ defines the thermal radiation parameter, $\gamma = \phi' \big/ h$ and $\sigma = \phi'' \big/ h$ shows the cold and heated wall slip parameters respectively.

## 3. Entropy Production

In dimensional format, the entropy configuration is written as

$$E'''_{gen} = \frac{k_{hnf}}{T_0^2}\left(\frac{\partial T'}{\partial y'}\right)^2 + \frac{\mu_{hnf}}{T_0}\left(\frac{\partial u'}{\partial y'}\right)^2 + \frac{\mu_{hnf}}{T_0}\left(u'\right)^2, \tag{17}$$

The preceding equation can be divided into three segments. The first part shows the irreversibility owing to heat transmission, the second part shows the unsustainability because of the fluid friction, and the third and final part indicates porosity characteristics. By using non-dimensional parameters in the above equation, we get the entropy equation as

$$N_S = \frac{E'''_{gen}}{E'''_g} = A_5\left(\frac{\partial \theta}{\partial y}\right)^2 + A_2 \frac{Br}{\Omega}\left(\frac{\partial u}{\partial y}\right)^2 + A_2 \frac{Br}{\Omega} Su^2, \tag{18}$$

where

$$E'''_g = \frac{k_f\left(T_0 - T_1\right)}{T_0 h^2}, \quad and \quad \Omega = \frac{T_0 - T_1}{T_0}. \tag{29}$$

For the existing derivation, the Bejan number is defined as

$$Be = \frac{A_5\left(\frac{\partial \theta}{\partial y}\right)^2}{A_5\left(\frac{\partial \theta}{\partial y}\right)^2 + A_2 \frac{Br}{\Omega}\left(\frac{\partial u}{\partial y}\right)^2 + A_2 \frac{Br}{\Omega} Su^2}. \tag{20}$$

## 4. Exact solutions

To solve the equations (14) and (15) with boundary conditions given in equation (16), we consider the solution in the form

$$\lambda = \lambda_0 + \lambda_1 e^{i\omega t}, \quad u\left(t, y\right) = \frac{\delta y}{\delta x}\tilde{B}\left(y\right)e^{i\omega t} + \tilde{A}\left(y\right), \quad \theta\left(t, y\right) = e^{i\omega t}\tilde{F}\left(y\right) + \tilde{E}\left(y\right). \tag{21}$$

Replacing the aforementioned equation (21) into equations (14) through (16), we obtain the following equations.

$$A_2\tilde{A}''\left(y\right) - \left(A_2 S^2 + A_3 H^2\right)\tilde{A}\left(y\right) = -\lambda_0, \tag{22}$$

$$A_2\tilde{B}''\left(y\right) - \left(A_3 H^2 + A_2 S^2 + A_1 \operatorname{Re} i\omega\right)\tilde{B}\left(y\right) = -\lambda_1, \tag{23}$$

$$\alpha\tilde{E}''\left(y\right) + \beta Br\left(\tilde{A}'(y)\right)^2 = 0, \tag{24}$$

$$\alpha\tilde{F}''\left(y\right) - i\omega\tilde{F}\left(y\right) + 2\beta Br\tilde{A}'(y)\tilde{B}'\left(y\right) = 0. \tag{25}$$

subjected to suitable boundary conditions

$$\tilde{A}\left(0\right) = \gamma\tilde{A}'\left(0\right); \quad \tilde{A}\left(1\right) = \sigma\tilde{A}'\left(1\right), \quad \tilde{B}\left(0\right) = \gamma\tilde{B}'\left(0\right); \quad \tilde{B}\left(1\right) = \sigma\tilde{B}'\left(1\right), \tag{26}$$

$$\tilde{E}(0)=0; \qquad \tilde{E}(1)=1, \qquad \tilde{F}(0)=0; \qquad \tilde{F}(1)=(1). \tag{27}$$

By solving equations (23)-(26) together with equations (27) - (28), we get

$$\tilde{A}(y)=C_1 e^{\frac{-m_1 y}{\sqrt{A_2}}}+C_2 e^{\frac{m_1 y}{\sqrt{A_2}}}+\frac{\lambda_0}{m_1^2}, \tag{28}$$

$$\tilde{B}(y)=C_3 e^{\frac{-m_2 y}{\sqrt{A_2}}}+C_4 e^{\frac{m_2 y}{\sqrt{A_2}}}+\frac{\lambda_1}{m_2^2}, \tag{29}$$

$$\tilde{E}(y)=C_5+C_6 y+\frac{Br\beta\left(C_2^2 e^{\frac{-2ym_1}{\sqrt{A_2}}}+C_1^2 e^{\frac{2ym_1}{\sqrt{A_2}}}-C_1C_2\log\left[e^{\frac{2ym_1}{\sqrt{A_2}}}\right]^2\right)}{4\alpha}, \tag{30}$$

$$\tilde{F}(y)=C_7 e^{-m_5 y}+C_8 e^{m_5 y}-j_1 e^{m_3 y}-j_2 e^{-m_3 y}+j_3 e^{m_4 y}+j_4 e^{-m_4 y}. \tag{31}$$

where

$$C_1=-\frac{\left(\sqrt{A_2}\left(-\sqrt{A_2}+\sqrt{A_2}\,\mathrm{e}^{\frac{m_1}{\sqrt{A_2}}}+\mathrm{e}^{\frac{m_1}{\sqrt{A_2}}}\gamma m_1-\sigma m_1\right)\lambda_0\right)}{m_1^2\left(-A_2+A_2\mathrm{e}^{\frac{2m_1}{\sqrt{A_2}}}+\sqrt{A_2}\gamma m_1+\sqrt{A_2}\mathrm{e}^{\frac{2m_1}{\sqrt{A_2}}}\gamma m_1-\sqrt{A_2}\sigma m_1-\sqrt{A_2}\mathrm{e}^{\frac{2m_1}{\sqrt{A_2}}}\sigma m_1+\gamma\sigma m_1^2-\mathrm{e}^{\frac{2m_1}{\sqrt{A_2}}}\gamma\sigma m_1^2\right)},$$

$$C_2=\frac{\left(\sqrt{A_2}\mathrm{e}^{\frac{m_1}{\sqrt{A_2}}}\left(-\sqrt{A_2}+\sqrt{A_2}\mathrm{e}^{\frac{m_1}{\sqrt{A_2}}}+\gamma m_1-\mathrm{e}^{\frac{m_1}{\sqrt{A_2}}}\sigma m_1\right)\lambda_0\right)}{\left(\left(m_1^2\left(-A_2+A_2\mathrm{e}^{\frac{2m_1}{\sqrt{A_2}}}+\sqrt{A_2}\gamma m_1+\sqrt{A_2}\mathrm{e}^{\frac{2m_1}{\sqrt{A_2}}}\gamma m_1-\sqrt{A_2}\sigma m_1-\sqrt{A_2}\mathrm{e}^{\frac{2m_1}{\sqrt{A_2}}}\sigma m_1+\gamma\sigma m_1^2-\mathrm{e}^{\frac{2m_1}{\sqrt{A_2}}}\gamma\sigma m_1^2\right)\right)\right)},$$

$$C_3=-\frac{\sqrt{A_2}\left(-\sqrt{A_2}+\sqrt{A_2}\mathrm{e}^{\frac{m_2}{\sqrt{A_2}}}+\mathrm{e}^{\frac{m_2}{\sqrt{A_2}}}\gamma m_2-\sigma m_2\right)\lambda_1}{m_2^2\left(-A_2+A_2\mathrm{e}^{\frac{2m_2}{\sqrt{A_2}}}+\sqrt{A_2}\gamma m_2+\sqrt{A_2}\mathrm{e}^{\frac{2m_2}{\sqrt{A_2}}}\gamma m_2-\sqrt{A_2}\sigma m_2-\sqrt{A_2}\mathrm{e}^{\frac{2m_2}{\sqrt{A_2}}}\sigma m_2+\gamma\sigma m_2^2-\mathrm{e}^{\frac{2m_2}{\sqrt{A_2}}}\gamma\sigma m_2^2\right)},$$

$$C_4=-\frac{\sqrt{A_2}\mathrm{e}^{\frac{m_2}{\sqrt{A_2}}}\left(-\sqrt{A_2}+\sqrt{A_2}\mathrm{e}^{\frac{m_2}{\sqrt{A_2}}}+\gamma m_2-\mathrm{e}^{\frac{m_2}{\sqrt{A_2}}}\sigma m_2\right)\lambda_1}{m_2^2\left(-A_2+A_2\mathrm{e}^{\frac{2m_2}{\sqrt{A_2}}}+\sqrt{A_2}\gamma m_2+\sqrt{A_2}\mathrm{e}^{\frac{2m_2}{\sqrt{A_2}}}\gamma m_2-\sqrt{A_2}\sigma m_2-\sqrt{A_2}\mathrm{e}^{\frac{2m_2}{\sqrt{A_2}}}\sigma m_2+\gamma\sigma m_2^2-\mathrm{e}^{\frac{2m_2}{\sqrt{A_2}}}\gamma\sigma m_2^2\right)},$$

$$C_5=\frac{Br\left(C_1^{\,2}+C_2^{\,2}\right)\beta}{4\alpha},\ C_6=\frac{\mathrm{e}^{-\frac{2m_1}{\sqrt{A_2}}}\left(\begin{array}{l}4\mathrm{e}^{\frac{2m_1}{\sqrt{A_2}}}\alpha+BrC_2^{\,2}\beta-BrC_1^{\,2}\mathrm{e}^{\frac{2m_1}{\sqrt{A_2}}}\beta-BrC_2^{\,2}\mathrm{e}^{\frac{2m_1}{\sqrt{A_2}}}\beta\\+BrC_1^{\,2}\mathrm{e}^{\frac{4m_1}{\sqrt{A_2}}}\beta-BrC_1C_2\mathrm{e}^{\frac{2m_1}{\sqrt{A_2}}}\beta\log\left[\mathrm{e}^{\frac{2m_1}{\sqrt{A_2}}}\right]^2\end{array}\right)}{4\alpha},$$

$$C_7 = -\frac{-1-\mathrm{e}^{m_3} j_1 - \mathrm{e}^{-m_3} j_2 + \mathrm{e}^{m_4} j_3 + \mathrm{e}^{-m_4} j_4 - \mathrm{e}^{m_5}\left(-j_1 - j_2 + j_3 + j_4\right)}{\mathrm{e}^{-m_5} - \mathrm{e}^{m_5}},$$

$$C_8 = \frac{\mathrm{e}^{-m_3-m_4}\left(\begin{array}{l}\mathrm{e}^{m_3+m_4+m_5} - \mathrm{e}^{m_3+m_4} j_1 + \mathrm{e}^{2m_3+m_4+m_5} j_1 - \mathrm{e}^{m_3+m_4} j_2 + \mathrm{e}^{m_4+m_5} j_2 \\ +\mathrm{e}^{m_3+m_4} j_3 - \mathrm{e}^{m_3+2m_4+m_5} j_3 + \mathrm{e}^{m_3+m_4} j_4 - \mathrm{e}^{m_3+m_5} j_4\end{array}\right)}{-1+\mathrm{e}^{2m_5}},$$

$$j_1 = \frac{2*\beta*Br*m_1*m_2*C_1*C_3}{m_3{}^2 - m_5{}^2}, \quad j_2 = \frac{2*\beta*Br*m_1*m_2*C_4*C_2}{m_3{}^2 - m_5{}^2}, \quad j_3 = \frac{2*\beta*Br*m_1*m_2*C_1*C_4}{m_4{}^2 - m_5{}^2},$$

$$j_4 = \frac{2*\beta*Br*m_1*m_2*C_3*C_2}{m_4{}^2 - m_5{}^2}, \qquad m_1 = \sqrt{A_2*H^2 + A_3*S^2}, \qquad m_2 = \sqrt{A_3*H^2 + A_2*S^2 + \mathrm{i}*\omega*A_1 1},$$

$$m_3 = \frac{m_1+m_2}{\sqrt{A_2}}, \; m_4 = \frac{m_1-m_2}{\sqrt{A_2}}, \; m_5 = \sqrt{\frac{\omega}{\alpha}}*(-1)^{\frac{1}{4}}.$$

The impact of the dimensionless rate of heat transfer at the suction/injection walls of the channel is given below

$$Nu = \frac{-\partial\theta}{\partial y} = -C_6 + \frac{1}{4\alpha} Br\beta \left( -\frac{2C_2{}^2 \mathrm{e}^{-\frac{2ym_1}{\sqrt{A2}}} m_1}{\sqrt{A_2}} + \frac{2C_1{}^2 \mathrm{e}^{\frac{2ym_1}{\sqrt{A2}}} m_1}{\sqrt{A_2}} - \frac{4C_1C_2 \log\left[\mathrm{e}^{\frac{2ym_1}{\sqrt{A2}}}\right] m_1}{\sqrt{A_2}} \right) \tag{32}$$

$$-\mathrm{e}^{\mathrm{i}t\omega}\left(-\mathrm{e}^{ym_3} j_1 m_3 + \mathrm{e}^{-ym_3} j_2 m_3 + \mathrm{e}^{ym_4} j_3 m_4 - \mathrm{e}^{-ym_4} j_4 m_4 - C_7 \mathrm{e}^{-ym_5} m_5 + C_8 \mathrm{e}^{ym_5} m_5\right).$$

The skin friction of such type of nanofluid is given as

$$\tau = -\mu\frac{\partial u}{\partial y} = -A2\left( -\frac{C_2 \mathrm{e}^{-\frac{ym_1}{\sqrt{A2}}} m_1}{\sqrt{A_2}} + \frac{C_1 \mathrm{e}^{\frac{ym_1}{\sqrt{A2}}} m_1}{\sqrt{A_2}} + \mathrm{e}^{\mathrm{i}t\omega}\left( -\frac{C_4 \mathrm{e}^{-\frac{ym_2}{\sqrt{A2}}} m_2}{\sqrt{A_2}} + \frac{C_3 \mathrm{e}^{\frac{ym_2}{\sqrt{A2}}} m_2}{\sqrt{A_2}} \right)\right). \tag{33}$$

**5. Results and discussion**

The exact solution of the governing equations (23)-(26) subjected to the boundary conditions (27)-(28) are obtained through the integration technique. The impact of various important parameters, including the cold wall slip parameter, Hartman number, Darcy parameter, and heated wall slip parameter are analyzed on velocity and temperature properties through Figures 2-4. Figure 2a in the study demonstrates that increasing the cold wall slip parameter significantly boosts fluid velocity, indicating less resistance and enhanced flow characteristics. However, this adjustment has a minimal effect on the heated wall, suggesting that other factors may dominate there. The figure also contrasts the behavior of standard nanofluids and hybrid nanofluids under these conditions, highlighting the distinct responses due to different nanoparticle compositions. Figure 2b in the study demonstrates how the Hartmann number affects the flow profiles of standard and hybrid nanofluids, highlighting the influence of stronger magnetic fields which slow down the fluid due to the Lorentz force. Interestingly, wall slip at the upper wall causes a reverse flow, enhancing fluid velocity there. This interaction offers insights valuable for designing cooling systems, chemical processing, and medical devices involving controlled fluid flows under magnetic influence. Figure 2c reveals that increasing the porous permeability parameter leads to a decrease in the velocity profile, except near the injection wall where flow reverses, indicating enhanced fluid movement. The graph compares hybrid nanofluid and nanofluid, with the solid line representing nanofluid and the dashed line

representing hybrid nanofluid, highlighting differing fluid dynamics. A decrease in the flow profile as a result of higher slippage at the wall, leading to less drag and more fluid freedom, is depicted in Figure 2d, which shows the effect of raising the Navier slip parameter on channel fluid flow. It reveals diverse effects at various wall types, with the suction wall showing little influence and the injection wall showing a considerable increase in velocity because of slip circumstances. Microfluidics, cooling systems, and industrial fluid transport can all benefit from the insights provided by comparing nanofluid and hybrid nanofluid, which highlight the impact of differing nanoparticle compositions on flow behaviour under different slip situations.

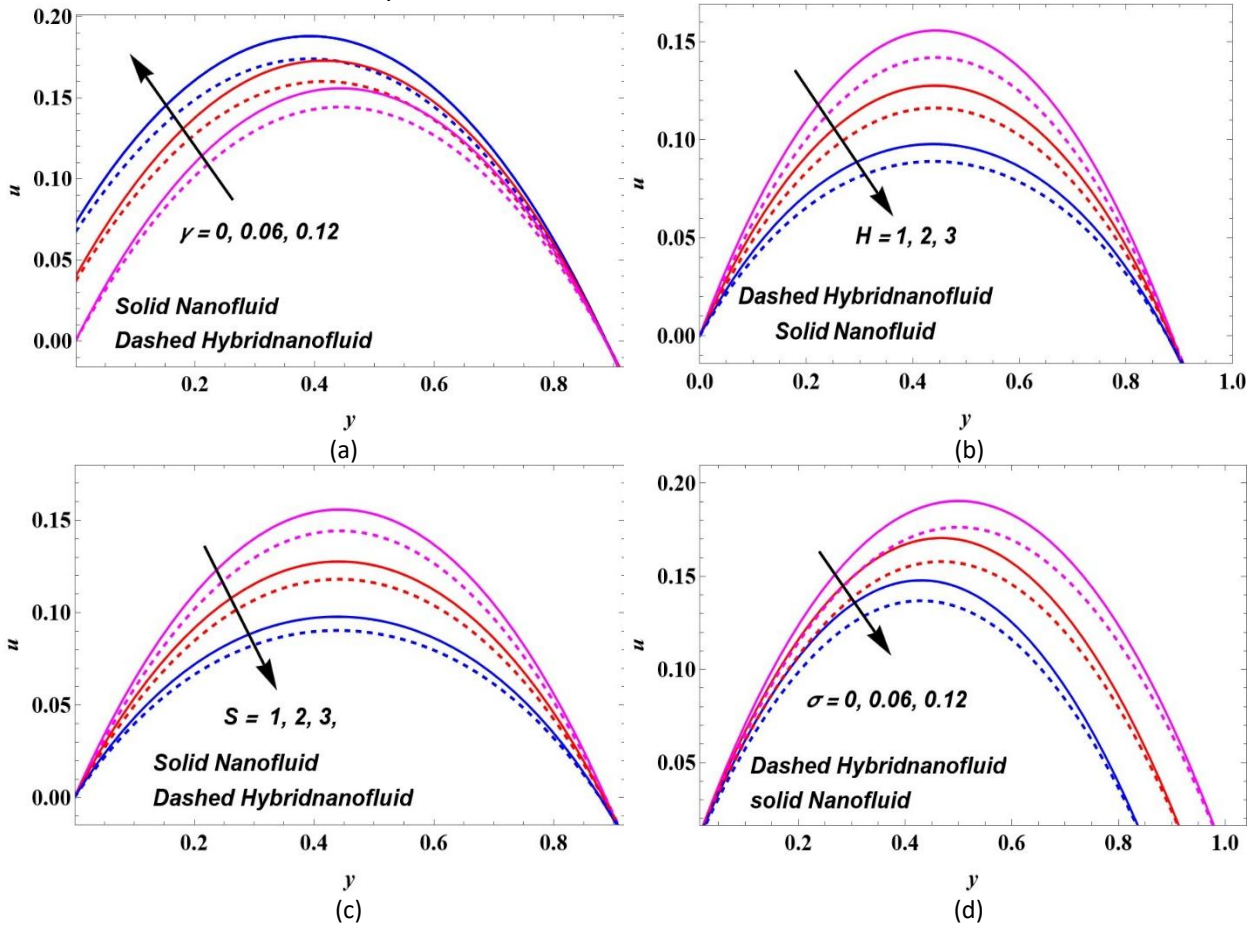


**Fig. 2.** Variations in velocity due to the (a) Navier slip parameter at the cold wall, (b) Hartman number (c) permeability parameter (d) Navier slip parameter at the heated wall

Figure 3a demonstrates how the Brinkmann number affects the temperature distribution. As the Brinkmann number grows, the temperature profile diminishes. The temperature drops more rapidly due to viscous dissipation, indicating slower heat conduction. The figure illustrates the contrasting behaviour of nanofluids and hybrid nanofluids. The solid line corresponds to nanofluids, while the dashed line corresponds to hybrid nanofluids. Figure 3b illustrates that higher radiation parameters result in elevated temperature profiles of fluids, as absorbed electromagnetic radiation is converted into heat. The impact is more prominent in hybrid nanofluids as opposed to ordinary nanofluids. Gaining a comprehensive understanding of this correlation is essential for enhancing the regulation of heat in various fields, including electronics cooling, industrial operations, solar energy systems, and aerospace engineering. Engineers can improve the efficiency and performance of fluids in high-temperature situations by optimizing radiation parameters. Figure 3c demonstrates that an increase in the porous permeability parameter leads to a decrease in skin friction, with the exception of the

injection wall where flow reversal takes place. The nanofluids (shown by the solid line) and hybrid nanofluids (represented by the dashed line) exhibit contrasting frictional characteristics, as shown in the comparison. This comprehension facilitates the optimization of fluid flow in applications involving porous media. Figure 3d demonstrates that the Nusselt number increases with the Brinkman number, indicating enhanced convective heat transfer due to greater viscous dissipation. Higher Brinkman numbers generate more internal heat, increasing the temperature gradient and thus the Nusselt number.

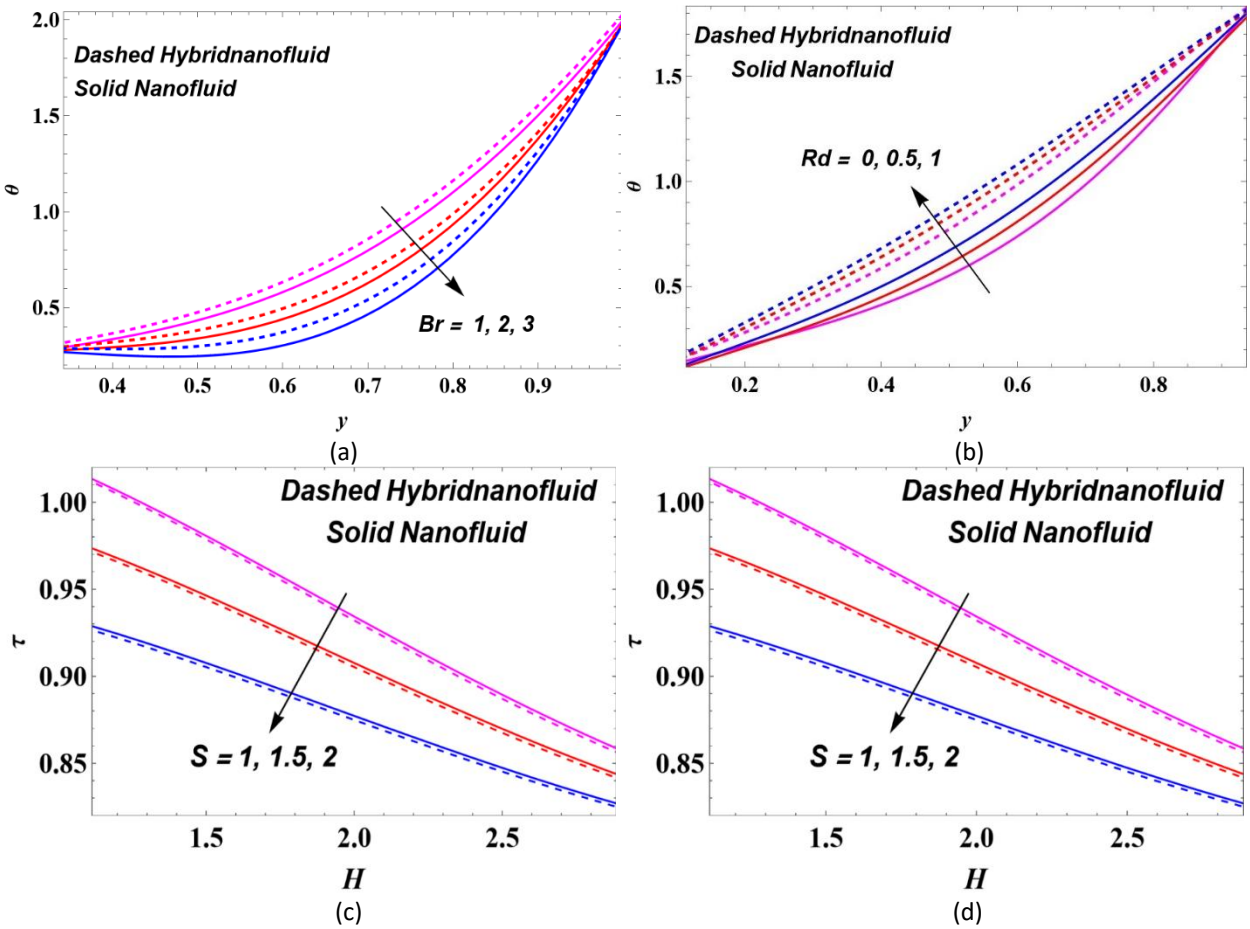


**Fig. 3.** Variations in temperature due to (a) Brikmann number (b) thermal radiation (c) skin friction due to porous permeability (d) Nusselt number due to Brinkman number

Figures 4a and 4b demonstrate that increasing the Brinkman number leads to higher entropy and Bejan numbers. The rise in the entropy profile is due to increased viscous dissipation, which generates additional heat within the fluid. This also elevates the temperature gradient, contributing to higher entropy generation. The Bejan number increases as fluid friction irreversibility becomes more significant than heat conduction irreversibility. Comparisons between standard nanofluids and hybrid nanofluids highlight how different nanoparticle compositions affect these thermodynamic parameters. These insights are crucial for optimizing the efficiency and performance of nanofluids in various applications. Figures 4c and 4d show how the entropy profile and Bejan number vary with the inverse of the Darcy parameter. Increasing the permeability parameter decreases the Entropy Profile while increasing the Darcy parameter (excluding the injection wall) increases it. Figure 4e demonstrates that the Bejan number increases with higher permeability, as it increases by decreasing the Darcy parameter, again excluding the injection wall. These comparisons highlight the differences between nanofluids and hybrid nanofluids in response to permeability changes. Figures 4e and 4f

illustrate the variation of the Entropy Profile and Bejan number with dimensionless temperature difference parameters. As the dimensionless temperature difference increases, the Entropy Profile decreases. Additionally, the Bejan number increases with the dimensionless temperature difference, as shown in Figure 4f. This figure also compares nanofluids (solid line) and hybrid nanofluids (dotted line), highlighting the distinct behaviors of these fluids under varying temperature differences.

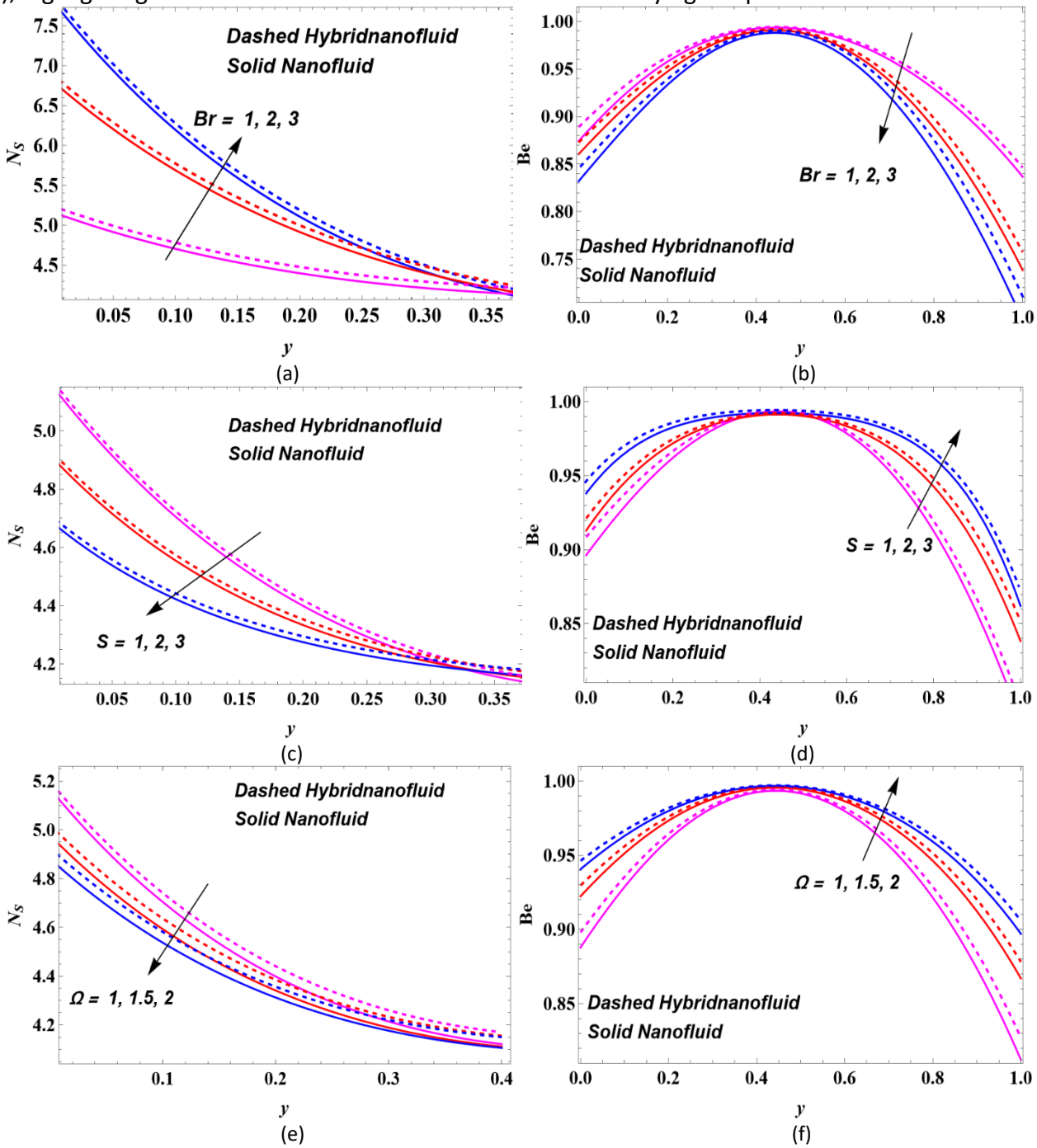


**Fig. 3.** Variations in entropy profile due to (a) Brikmann number (c) porous permeability parameter (e) temperature difference parameter, and in Bejan number (b) Brikmann number (d) porous permeability parameter (f) temperature difference parameter

Table 3 shows that increasing the Prandtl number enhances the heat profile rate at the suction wall, but reduces the Nusselt number at the injection wall. Table 4 indicates that skin friction

increases with higher values at both suction and injection walls. Table 5 concludes that increasing the heated wall slip parameter raises skin friction at both the cold and heated walls.

**Table 3**
Calculation showing the impact of the Prandtl number on the Nusselt number

| *y* | *Br* | *Pr* | *Nu* | *Pr* | *Nu* | *Pr* | *Nu* |
|---|---|---|---|---|---|---|---|
| 0. | 1 | 0.44 | -2.057085 | 0.71 | -2.057782 | 1 | -2.055786 |
| 0.25 | 1 | 0.44 | -2.010220 | 0.71 | -2.007497 | 1 | -2.002537 |
| 0.5 | 1 | 0.44 | -2.008439 | 0.71 | -2.008977 | 1 | -2.009380 |
| 0.75 | 1 | 0.44 | -1.994828 | 0.71 | -1.998022 | 1 | -2.003466 |
| 1 | 1 | 0.44 | -1.905278 | 0.71 | -1.901499 | 1 | -1.900584 |

**Table 4**
Calculation showing the impact of skin friction on cold wall slip

| *y* | σ | γ | τ | γ | τ | γ | τ |
|---|---|---|---|---|---|---|---|
| 0 | 0.1 | 0 | -0.783650 | 0.2 | -0.586519 | 0.3 | -0.520785 |
| 0.25 | 0.1 | 0 | -0.323756 | 0.2 | -0.176271 | 0.3 | -0.127254 |
| 0.5 | 0.1 | 0 | -0.093921 | 0.2 | 0.210782 | 0.3 | 0.249505 |
| 0.75 | 0.1 | 0 | 0.523816 | 0.2 | 0.625582 | 0.3 | 0.659237 |
| 1 | 0.1 | 0 | 1.021702 | 0.2 | 1.122157 | 0.3 | 1.155372 |

**Table 5**
Calculation showing the impact of skin friction on heated wall slip

| y | γ | σ | τ | σ | τ | σ | τ |
|---|---|---|---|---|---|---|---|
| 0 | 0.1 | 0 | -0.737739 | 0.1 | -0.671050 | 0.2 | -0.573436 |
| 0.25 | 0.1 | 0 | -0.314305 | 0.1 | -0.239423 | 0.2 | -0.130120 |
| 0.5 | 0.1 | 0 | 0.067720 | 0.1 | 0.160807 | 0.2 | 0.296045 |
| 0.75 | 0.1 | 0 | 0.458709 | 0.1 | 0.582099 | 0.2 | 0.760393 |
| 1 | 0.1 | 0 | 0.910037 | 0.1 | 1.079238 | 0.2 | 1.322385 |

## 6. Conclusions

Nanofluids are extensively utilized in biomedical engineering and various industries for applications like heat exchangers, engine cooling, cancer treatments, and nano-drug delivery. This article investigates the effects of variable viscosity and thermal conductivity on the hydromagnetic pulsatile flow of hybrid nanoliquid through a horizontal porous channel. Entropy generation is also carried out. The impact of different physical parameters on flow variables is depicted through graphs and tables. Key findings highlighted significant impacts.

- The impact of the cold wall slip parameter increasing is an escalation in fluid velocity.
- Reduced fluid velocity is associated with an upsurge in the Hartmann number.
- Increasing the permeability of the porous medium leads to a reduction in fluid velocity.
- No slip is found at a heated wall, when σ = 0, and a slight and pronounced reduction in the velocity at heated walls is found by enhancing in σ.
- This article reveals oscillating temperature and velocity profiles when comparing hybrid nanofluid and nanofluid.
- The temperature profile decreases by increasing the Brinkmann number.
- The rate of heat transport escalates by elevating the thermal radiation.
- Entropy increases with Brinkman number and decreases with temperature difference.

- The Bejan number decreases with the Brinkman number and increases with temperature difference and permeability.

**Author Contributions**

Conceptualization, M.Y.R., Z. A.; methodology, G.M., M.S.A.; software, M.S.A.; validation, J.H., M.Y.R., formal analysis, J.H.; investigation, G.M., M.SA.; writing—original draft preparation, M.Y.R., M.S.A.; writing—review and editing, J.H., M.Y.R; supervision, Z.A.; project administration, Z.A. All authors have read and agreed to the published version of the manuscript.

**Funding**

This research received no external funding.

**Data Availability Statement**

The data that support the findings of this study are available on request from the corresponding author.

**Conflicts of Interest**

The authors declare that they have no known competing financial interests or personal relationships that could have appeared to influence the work reported in this paper.

**Acknowledgement**

N/A.

**References**

[1] Makinde, O. D., and Mhone, P. Y. (2005) Heat transfer to MHD oscillatory flow in a channel filled with porous medium. Romanian Journal of Physics, 50(9/10), 931.

[2] Mehmood, A., and Ali, A. (2007) The effect of slip condition on unsteady MHD oscillatory flow of a viscous fluid in a planer channel. Romanian Journal of Physics, 52(1/2), 85.

[3] Hakeem, A. A., and Sathiyanathan, K. (2009) An analytic solution of an oscillatory flow through a porous medium with radiation effect. Nonlinear Analysis Hybrid System, 3(3), 288-295 https://doi.org/10.1016/j.nahs.2009.01.011

[4] Jha, B. K., and Ajibade, A. O. (2009) Free convective flow of heat generating/absorbing fluid between vertical porous plates with periodic heat input. International Communications in Heat and Mass Transfer. 36(6), 624-631. http://dx.doi.org/10.1016/j.icheatmasstransfer.2009.03.003

[5] Jha, B. K., and Ajibade, A. O. (2010) Free convective flow between vertical porous plates with periodic heat input. ZAMM-Journal of Applied Mathematics and Mechanic: Applied Mathematics and Mechanics, 90(3), 185-193. https://doi.org/10.1002/zamm.200900268

[6] Jha, B. K., & Ajibade, A. O. (2012). Effect of viscous dissipation on natural convection flow between vertical parallel plates with time-periodic boundary conditions. Communications in Nonlinear Science and Numerical Simulation. 17(4), 1576-1587. https://doi.org/10.1016/j.cnsns.2011.09.020

[7] Umavathi, J. C., Chamkha, A. J., Mateen, A., and Al-Mudhaf, A. (2009). Unsteady oscillatory flow and heat transfer in a horizontal composite porous medium channel. Nonlinear Analysis: Modelling and Control., 14(3), 397-415. https://doi.org/10.15388/NA.2009.14.3.14503

[8] Yuan, J., and Wang, D. (2019) An experimental investigation of acceleration-skewed oscillatory flow over vortex ripples. Journal of Geophysical Research: Oceans. 124(12), 9620-9643. https://doi.org/10.1029/2019JC015487

[9] Earnshaw, H.C., Greated, C.A., 1998. Dynamics of ripple bed vortices. Experiments in Fluids. 25 (3), 265–275. https://doi.org/10.1007/s003480050229

[10] Malarkey, J., & Davies, A. G. (2002). Discrete vortex modeling of oscillatory flow over ripples. Applied Ocean Research. 24(3), 127-145. https://doi.org/10.1016/S0141-1187(02)00035-4

[11] Chen, X., & Yu, X. (2015). A numerical study on oscillatory flow-induced sediment motion over vortex ripples. Journal of Physical Oceanography. 45(1), 228-246. https://doi.org/10.1175/JPO-D-14-0031.1

[12] Hu, T., Ren, H., Shen, J., Niu, Z., Zhang, M., Xu, Y., and Sun, T. (2023) Experimental investigation on hydrodynamic forces of semi-submerged cylinders in combined steady flow and oscillatory flow. Ocean Engineering. 268, 113612. https://doi.org/10.1016/j.oceaneng.2022.113612

[13] Ja'fari, M., and Jaworski, A. J. (2023) On the nonlinear behavior of oscillatory flow in a high-pressure amplitude standing-wave thermoacoustic heat engine International Journal of Heat and Mass Transfer. 201, 123595. https://doi.org/10.1016/j.ijheatmasstransfer.2022.123595

[14] Niyas, M. M., and Shaija, A. (2023) Biodiesel production from coconut waste cooking oil using novel solar powered rotating flask oscillatory flow reactor and its utilization in diesel engine. Thermal Science and Engineering Progress 40, 101794. https://doi.org/10.1016/j.tsep.2023.101794

[15] Bala Anasuya, J., and Srinivas, S. (2023) Heat transfer characteristics of magnetohydrodynamic two fluid oscillatory flow in an inclined channel with saturated porous medium. Proceedings of the Institution of Mechanical Engineers, Part E: Journal of Process Mechanical Engineering. 2024;238(1):427-440. https://doi.org/10.1177/09544089221146364

[16] Choi, S. U., and Eastman, J. A. (1995) Enhancing thermal conductivity of fluids with nanoparticles (No. ANL/MSD/CP-84938; CONF-951135-29). Argonne National Lab. (ANL), Argonne, IL (United States).

[17] Kirubadurai, B., Selvan, P., Vijayakumar, V., and Karthik, M. (2014) Heat transfer enhancement of nanofluids–a Review Int Res J Eng Technol. 3(07), 483-486. https://doi.org/10.1016/j.rser.2009.10.004

[18] Bang, I. C., and Chang, S. H. (2005) Boiling heat transfer performance and phenomena of Al2O3–water nano-fluids from a plain surface in a pool. International Journal of Heat and Mass Transfer 48(12), 2407-2419. http://dx.doi.org/10.1016/j.ijheatmasstransfer.2004.12.047

[19] Nallusamy, S., Babu, A. M., and Prabu, N. M. (2015) Investigation on carbon nanotubes over review on other heat transfer nanofluids. International Journal of Applied Engineering Research. 10(62), 112-117.

[20] Suresh, S., Venkitaraj, K. P., Selvakumar, P., and Chandrasekar, M. (2012) Effect of Al2O3–Cu/water hybrid nanofluid in heat transfer. Experimental Thermal and Fluid Science 38, 54-60. https://doi.org/10.1016/j.expthermflusci.2011.11.007

[21] Hayat, T., and Nadeem, S. (2017) Heat transfer enhancement with Ag–CuO/water hybrid nanofluid. Results in Physics. 7, 2317-2324. https://doi.org/10.1016/j.rinp.2017.06.034

[22] Madhesh, D., & Kalaiselvam, S. (2014). Experimental analysis of hybrid nanofluid as a coolant. Procedia Engineering. 97, 1667-1675. https://doi.org/10.1016/j.proeng.2014.12.317

[23] Ahmadi, M. H., Mirlohi, A., Nazari, M. A., and Ghasempour, R. (2018) A review of thermal conductivity of various nanofluids. Journal of Molecular Liquid. 265, 181-188. http://dx.doi.org/10.1016/j.molliq.2018.05.124

[24] Subhani, M., and Nadeem, S. (2019) Numerical analysis of micropolar hybrid nanofluid. Applied Nanoscience, 9(4), 447-459. https://doi.org/10.1007/s13204-018-0926-2

[25] Saleem, A., Akhtar, S., and Nadeem, S. (2022) Bio-mathematical analysis of electro-osmotically modulated hemodynamic blood flow inside a symmetric and nonsymmetric stenosed artery with joule heating. International Journal of Biomathematics. 15(02), 2150071. https://doi.org/10.1142/S1793524521500716

[26] Shahzad, M. H., Awan, A. U., Akhtar, S., and Nadeem, S. (2022) Entropy and stability analysis on blood flow with nanoparticles through a stenosed artery having permeable walls. Science Progress. 105(2). doi:10.1177/00368504221096000

[27] Tang, T., and Gao, H. (2016) Strong solutions to 3D compressible magnetohydrodynamic equations with Navier-slip condition. Mathematial Methods in the Applied Sciences, 39(10), 2768-2782. https://doi.org/10.1002/mma.3734

[28] Xi, S., and Hao, X. (2017) Existence of the compressible magnetohydrodynamic equations with vacuum. Journal of Mathematical Analysis and Applications. 453(1), 410-433. https://doi.org/10.1016/j.jmaa.2017.04.007

[29] Cai, G., and Li, J. (2021) Existence and exponential growth of global classical solutions to the compressible Navier-Stokes equations with slip boundary conditions in 3D bounded domains. Indiana University Mathematics Journal, 72(6), 2491-2546. http://dx.doi.org/10.1512/iumj.2023.72.9591